

# Redshift-space fluctuations in stochastic gravitational wave background

Kin-Wang Ng<sup>1,2</sup>

<sup>1</sup>*Institute of Physics, Academia Sinica, Taipei 11529, Taiwan*

<sup>2</sup>*Institute of Astronomy and Astrophysics, Academia Sinica, Taipei 11529, Taiwan*

(Dated: September 21, 2021)

We study the redshift-space fluctuations induced by a stochastic gravitational wave background via the Sachs-Wolfe effect. The redshift-space fluctuations can be encapsulated in a line-of-sight integral that is useful for studying the imprint of short-wavelength gravitational waves on the CMB anisotropy, as well as providing us with a precise redshift fluctuation correlation between a pair of pulsars in pulsar timing measurements.

## I. INTRODUCTION

The search for stochastic gravitational wave background (SGWB) is one of the main goals in observational cosmology. After the discovery of GWs emitted by a binary black hole merger made by the LIGO-Virgo Collaboration [1] and the observation of a handful of GW events from compact binary coalescences [2], the detection of the SGWB becomes the next milestone in a new era of GW astronomy and cosmology. There have been many studies on possible astrophysical and cosmological sources for the SGWB such as distant compact binary coalescences, early-time phase transitions, cosmic string or defect networks, second-order primordial scalar perturbations, and inflationary GWs [3]. GWs have very weak gravitational interaction, so they decouple from matter at the time of production and travel to us almost without being disturbed. At present, they remain as a GW background that encodes the information of the production processes in the early Universe.

The spectrum of the SGWB is expected to span a wide range of frequencies. The method adopted in the GW interferometry such as the LIGO-Virgo experiment for detecting the SGWB is to correlate the responses of a pair of detectors to the GW strain amplitude. The correlation allows us to filter out detector noises and obtain a large signal-to-noise ratio for the detection of GWs of frequencies at several tens hertz [3]. An indirect method to search for the SGWB is through their gravitational effects on physical observables such as the cosmic microwave background (CMB) [4] and the arrival times of radio pulses from millisecond pulsars [3]. Horizon-sized GWs can leave an imprint on the anisotropy and polarization of the CMB that has been long sought after in CMB experiments, whereas the pulsar timing is sensitive to short-wavelength GWs at nanohertz frequencies. Future GW experimental plans such as Einstein Telescope, Cosmic Explorer, LISA, DECIGO, Taiji, TianQin, international pulsar-timing arrays, and SKA [5], hand in hand with CMB Stage-4 experiments [6], will certainly bring

us a precision science in SGWB observation.

In this paper, we will give a systematic study of the gravitational effects induced by the SGWB on astrophysical and cosmological observables. In the next section, we firstly review the propagation of free GWs in the expanding universe. In Sec. III, the effect on the redshift space due to the presence of a SGWB is discussed. Then, this is applied to the induced CMB anisotropy in Sec. IV and pulsar timing in Sec. V. Section VI is our conclusion.

## II. STOCHASTIC GRAVITATIONAL WAVE BACKGROUND

Consider a perturbed metric:

$$ds^2 = -a^2 d\eta^2 + a^2 (\delta_{ij} + h_{ij}) dx^i dx^j, \quad (1)$$

where  $a(\eta)$  is the cosmic scale factor and  $\eta$  is the conformal time defined by  $d\eta = dt/a$ . The transverse-traceless tensor perturbation  $h_{ij}$  can be decomposed into two independent polarization tensors as

$$h_{ij}(\eta, \vec{x}) = \sum_{\lambda} \int \frac{d^3 \vec{k}}{(2\pi)^{\frac{3}{2}}} \left[ a_{\lambda}(\vec{k}) h_{\lambda}(\eta, \vec{k}) \epsilon_{ij}^{\lambda}(\hat{k}) e^{i\vec{k} \cdot \vec{x}} + H.c. \right], \quad (2)$$

where  $\epsilon_{ij}^{\lambda}(\hat{k}) \epsilon_{ij}^{\lambda'}(\hat{k}) = 2\delta_{\lambda\lambda'}$ . The annihilation and creation operators,  $a_{\lambda}(\vec{k})$  and  $a_{\lambda}^{\dagger}(\vec{k})$  respectively, satisfy the commutation relation,

$$\left[ a_{\lambda}(\vec{k}), a_{\lambda'}^{\dagger}(\vec{k}') \right] = \delta(\vec{k} - \vec{k}') \delta_{\lambda\lambda'}. \quad (3)$$

The GW amplitude,  $h_{\lambda}(\eta, \vec{k})$ , is governed by the equation of motion,

$$\frac{d^2 h_{\lambda}}{d\eta^2} + \frac{2}{a} \frac{da}{d\eta} \frac{dh_{\lambda}}{d\eta} + k^2 h_{\lambda} = 0. \quad (4)$$

The spectral energy density of the SGWB relative to the critical density is then given by

$$\Omega_{\text{GW}}(\eta, k, \hat{k}) \equiv \frac{k}{\rho_c} \frac{d\rho_{\text{GW}}}{dkd^2\hat{k}} = \sum_{\lambda} \frac{1}{12a^2H^2} \left(\frac{k}{2\pi}\right)^3 \times \left[ k^2 |h_{\lambda}|^2 + \left| \frac{dh_{\lambda}}{d\eta} \right|^2 \right], \quad (5)$$

where  $\rho_c = 3M_p^2H^2$ , with  $M_p$  being the reduced Planck mass. Writing  $h_{\lambda} = k^{-3/2}h$ , we have

$$\Omega_{\text{GW}}(\eta, k, \hat{k}) = \frac{1}{48\pi^3} \left(\frac{k}{aH}\right)^2 \left[ |h|^2 + \left| \frac{1}{k} \frac{dh}{d\eta} \right|^2 \right], \quad (6)$$

and the tensor power spectrum is defined as  $\mathcal{P}(\eta, k) \equiv |h(\eta, \vec{k})|^2 / (2\pi^2)$ . The  $h(\eta, \vec{k})$  is dispersive and it can be cast into  $h(\eta, \vec{k}) = h(k\eta)$ . For a superhorizon mode with  $k\eta \ll 1$ ,  $h(k\eta)$  has a constant amplitude;  $h(k\eta)$  then oscillates with a decaying envelope once the mode enter the horizon. For example, in slow-roll inflation models, metric quantum fluctuations during inflation give rise to an initial condition of the GW amplitude for superhorizon modes:

$$|h(k\eta)| = \frac{H_I}{M_p} \quad \text{for } k\eta \ll 1, \quad (7)$$

where  $H_I$  is the Hubble scale in inflation. This implies a scale-invariant power spectrum,

$$\mathcal{P}(k) \equiv \mathcal{P}(\eta, k)|_{k\eta \ll 1} = \frac{1}{2\pi^2} \frac{H_I^2}{M_p^2}. \quad (8)$$

Another kind of the SGWB may be generated in a physical process taking place within the horizon with a characteristic frequency  $k_*$  at time  $\eta_*$ :

$$|h(k_*\eta_*)| = \frac{H_*}{M_p} \quad \text{with } k_*\eta_* > 1, \quad (9)$$

where  $H_*$  represents some energy scale. This results in a narrow initial power spectrum with a peak height:

$$\mathcal{P}(\eta_*, k_*) = \frac{1}{2\pi^2} \frac{H_*^2}{M_p^2}. \quad (10)$$

The subsequent time evolution of  $h(k_*\eta)$  is then determined by Eq. (4) for  $\eta > \eta_*$ . The solution for this subhorizon mode can be approximated as

$$h(k_*\eta) \simeq \frac{H_*}{M_p} \frac{a(\eta_*)}{a(\eta)} e^{-ik_*\eta}. \quad (11)$$

From Eq. (6), the present spectral energy density for an isotropic SGWB is

$$\Omega_{\text{GW}} \simeq \frac{1}{6\pi^2} \frac{H_*^2}{M_p^2} \left[ \frac{k_* a(\eta_*)}{k_0 a(\eta_0)} \right]^2, \quad (12)$$

where  $k_0 = a(\eta_0)H_0$  is the wavenumber of the mode that just crosses the present horizon.

### III. REDSHIFT-SPACE FLUCTUATIONS

The gravitational effects due to the presence of a SGWB can be encoded in a fluctuation in the redshift of an observed photon source. Suppose the photon source locate at redshift  $z$ . Then, the fluctuation in the redshift of the photon source is given by the Sachs-Wolfe effect [7],

$$z + 1 = \frac{a(\eta_r)}{a(\eta_e)} \left[ 1 - \frac{1}{2} \int_{\eta_e}^{\eta_r} d\eta e^i e^j \frac{\partial}{\partial \eta} h_{ij}(\eta, \vec{x}) \right], \quad (13)$$

where  $\mathbf{e}$  is the propagation direction of the photon. The lower (upper) limit of integration in the line-of-sight integral represents the point of emission (reception) of the photon. Let  $\bar{z}$  be the mean redshift and  $\delta z = z - \bar{z}$  be the fluctuation. Then, we have  $1 + \bar{z} = a(\eta_r)/a(\eta_e)$  and

$$\Delta z(\mathbf{e}) \equiv \frac{\delta z}{1 + \bar{z}}(\mathbf{e}) = -\frac{1}{2} \int_{\eta_e}^{\eta_r} d\eta e^i e^j \frac{\partial}{\partial \eta} h_{ij}(\eta, \vec{x}). \quad (14)$$

This redshift-space fluctuation can be expanded in terms of spherical harmonics,

$$\Delta z(\mathbf{e}) = \sum_{l,m} a_{lm} Y_{lm}(\mathbf{e}). \quad (15)$$

For an isotropic unpolarized SGWB, the isotropy in the mean guarantees that

$$\langle a_{lm}^\dagger a_{l'm'} \rangle = C_l \delta_{ll'} \delta_{mm'}, \quad (16)$$

where  $C_l$  is the redshift-space anisotropy power spectrum, from which we can construct the two-point correlation function,

$$\langle \Delta z(\mathbf{e}_1) \Delta z(\mathbf{e}_2) \rangle = \sum_l \frac{2l+1}{4\pi} C_l P_l(\mathbf{e}_1 \cdot \mathbf{e}_2), \quad (17)$$

where  $P_l$  is the Legendre polynomial. Using Eq. (2) and doing the tensor contraction, we obtain the formula for the power spectrum as [8]

$$C_l = \frac{1}{2\pi} (l+2)(l+1)l(l-1) \times \int_0^\infty \frac{dk}{k} \left| \int_{\eta_e}^{\eta_r} d\eta \frac{dh(k\eta)}{d\eta} \frac{j_l[k(\eta_r - \eta)]}{k^2(\eta_r - \eta)^2} \right|^2, \quad (18)$$

where  $j_l$  is a spherical Bessel function.

### IV. CMB TEMPERATURE ANISOTROPY

The redshift-space fluctuations can induce a temperature anisotropy of the CMB, given by Eq. (14)

$$\frac{\delta T}{T}(\mathbf{e}) = \Delta z(\mathbf{e}), \quad (19)$$

where  $\eta_e = \eta_{\text{dec}}$  denoting the CMB decoupling time and  $\eta_r = \eta_0$  the present time. This is the well-known Sachs-Wolfe tensor contribution to the CMB temperature anisotropy, whose power spectrum is then given by Eq. (18).

### A. A scale-invariant power spectrum

The CMB temperature anisotropy due to the primordial tensor power spectrum (8) has been well studied (see, for example, Ref. [8]). For a fixed  $l$ , the main contribution to the integral (18) for  $C_l$  comes from the mode of wavenumber  $k \simeq l/\eta_0$  at the horizon crossing time  $\eta_c \simeq \pi/k$  [9]. Since a mode is dispersive after entering the horizon, the modes that can imprint a large anisotropy on the CMB should have  $\eta_c > \eta_{\text{dec}}$ . In the standard  $\Lambda$ CDM model [10],  $\eta_{\text{dec}} \simeq 300$  Mpc and the comoving distance to the CMB decoupling surface is  $\eta_0 - \eta_{\text{dec}} \simeq \eta_0 \simeq 14000$  Mpc. This explains why super-horizon modes with  $k < \pi/\eta_{\text{dec}} \simeq 0.01$  Mpc $^{-1}$  dominate the contribution to the CMB temperature anisotropy on large angular scales at  $l < \pi\eta_0/\eta_{\text{dec}} \simeq 150$ .

### B. A narrow power spectrum

For the narrow power spectrum (10), we adopt the subhorizon-mode solution (11),

$$h(k_*\eta) \simeq \frac{H_*}{M_p} \frac{1}{a(\eta)} e^{-ik_*\eta}, \quad (20)$$

where we have set  $a(\eta_*) = 1$  for our convenience. The induced CMB anisotropy power spectrum is

$$C_l \simeq \frac{1}{2\pi} (l+2)(l+1)l(l-1) \times \left| \Delta \ln k_* \left| \int_{\eta_1}^{\eta_0} d\eta \frac{dh(k_*\eta)}{d\eta} \frac{j_l[k_*(\eta_0 - \eta)]}{k_*^2(\eta_0 - \eta)^2} \right|^2 \right., \quad (21)$$

where  $\eta_1 = \max(\eta_{\text{dec}}, \eta_*)$ . Assuming that the spectrum spans a range of  $\Delta \ln k_* \simeq 1$  and that the universe was in a matter-dominated epoch with  $a(\eta) = (\eta/\eta_*)^2$ , we obtain

$$C_l \simeq \frac{k_*^4 \eta_*^4 H_*^2}{2\pi M_p^2} (l+2)(l+1)l(l-1) \times \left| \int_0^{x_1} dx \frac{(x_0 - x) - 2i}{(x_0 - x)^3} e^{ix} \frac{j_l(x)}{x^2} \right|^2, \quad (22)$$

where  $x = k_*(\eta_0 - \eta)$ ,  $x_0 = k_*\eta_0$ , and  $x_1 = k_*(\eta_0 - \eta_1)$ . We discuss the power spectrum in two limiting cases:

#### 1. $x_1 \lesssim x_0$

Let  $\eta_* < \eta_{\text{dec}}$ ; then  $x_1/x_0 = 137/140$ . For example, we have numerically computed the integral in Eq. (22) to obtain  $C_l$  for  $k_* = 0.14$  Mpc $^{-1}$ . We have found that the power spectrum  $l(l+1)C_l$  peaks around  $l \sim x_0 = 1960$ , as expected for the short-wavelength modes that mainly contribute to the small-scale anisotropy. In addition,  $l(l+1)C_l$  has a local maximum at  $l = 2$  and a local minimum at  $l = 21$ . This reproduces within an overall constant

factor the power spectrum found by using the CAMB numerical code [11]. It is interesting to note that short-wavelength GWs can contribute to the large-scale CMB anisotropy when the CMB photons arrive at the observer at the present epoch. This contribution is resulted from taking the limit,  $j_l(x)/x^2 \rightarrow x^{l-2}$  as  $x \rightarrow 0$ , in Eq. (22).

The numerical calculations of the integral (22), whose integrand is consisted of oscillating functions, meet heavy cancellation for  $k_* > 0.14$  Mpc $^{-1}$ . Thus, for high- $l$  multipoles, we let  $x = (l+1/2)y$  and approximate Eq. (22) as

$$C_l \simeq \frac{H_*^2}{4M_p^2} \left( \frac{\eta_*}{\eta_0} \right)^4 (l+2)(l+1)l(l-1)(l+1/2)^2 \times \left| \int_0^{y_1} dy \frac{1-x/x_0 - i2/x_0}{(1-x/x_0)^3} e^{ix} \frac{J_{l+\frac{1}{2}}[(l+\frac{1}{2})y]}{x^{5/2}} \right|^2, \quad (23)$$

where  $J_\nu(\nu y)$  takes the asymptotic form for a large order as

$$J_\nu(\nu y) \sim \frac{e^{\nu(1-y^2)^{\frac{1}{2}} - \nu \tanh^{-1}(1-y^2)^{\frac{1}{2}}}}{\sqrt{2\pi\nu} (1-y^2)^{\frac{1}{4}}} \quad \text{for } 0 < y < 1, \quad (24)$$

$$J_\nu(\nu y) \sim \frac{\cos[\nu(y^2-1)^{\frac{1}{2}} - \nu \tan^{-1}(y^2-1)^{\frac{1}{2}} - \pi/4]}{\sqrt{\pi\nu/2} (y^2-1)^{\frac{1}{4}}} \quad \text{for } y > 1. \quad (25)$$

We have found that this approximation works fairly well for high- $l$   $C_l$ 's.

#### 2. $x_1 \ll x_0$

In this case, it requires that  $\eta_* > \eta_{\text{dec}}$  and the power spectrum can be approximated as

$$C_l \simeq \frac{H_*^2}{2\pi M_p^2} \left( \frac{\eta_*}{\eta_0} \right)^4 (l+2)(l+1)l(l-1) \times \left| \int_0^{x_1} dx \left( 1 + \frac{2x}{x_0} + \frac{3x^2}{x_0^2} + \dots \right) e^{ix} \frac{j_l(x)}{x^2} \right|^2, \quad (26)$$

When  $x_1 \ll 1$ , we have

$$C_l \simeq \frac{H_*^2}{2\pi M_p^2} \left( \frac{\eta_*}{\eta_0} \right)^4 \frac{(l+2)(l+1)l(l-1)}{(2l+1)!!(2l+1)!!} x_1^{2l-2}. \quad (27)$$

When  $x_1 \gg 1$ , using the integral result,

$$\int_0^\infty dx e^{-\alpha x} J_\nu(\beta x) x^{\mu-1} = \frac{(\beta/2)^\nu \Gamma(\nu+\mu)}{\alpha^{\nu+\mu} \Gamma(\nu+1)} \times F\left(\frac{\nu+\mu}{2}, \frac{\nu+\mu+1}{2}; \nu+1; -\frac{\beta^2}{\alpha^2}\right), \quad (28)$$

where  $F(a, b; c; d)$  is a hypergeometric function which has a particular value,

$$F(a, b; c; 1) = \frac{\Gamma(c)\Gamma(c-a-b)}{\Gamma(c-a)\Gamma(c-b)}, \quad (29)$$

and the doubling formula for gamma functions,

$$\Gamma(2z) = \frac{2^{2z-1}}{\sqrt{\pi}} \Gamma(z) \Gamma(z + 1/2), \quad (30)$$

we obtain

$$\begin{aligned} & \int_0^{x_1} dx e^{ix} j_l(x) x^{\mu-1/2} \\ & \simeq \sqrt{\frac{\pi}{2}} \int_0^\infty dx e^{ix} J_{l+\frac{1}{2}}(x) x^{\mu-1} \\ & = \frac{i^{l+\mu+\frac{1}{2}}}{2^{\mu+\frac{1}{2}}} \Gamma(1/2 - \mu) \frac{\Gamma(l + \mu + 1/2)}{\Gamma(l - \mu + 3/2)}, \end{aligned} \quad (31)$$

where  $\alpha = -i$ ,  $\beta = 1$ ,  $\nu = l + 1/2$ , and we have approximated  $x_1$  by an infinity. Under this approximation, we keep only the first and the second terms in Eq. (26) that correspond to  $\mu = -3/2$  and  $-1/2$ , respectively. Hence, we have

$$C_l \simeq \frac{2H_*^2}{\pi M_p^2} \left( \frac{\eta_*}{\eta_0} \right)^4 \left[ \frac{1}{(l+2)(l+1)l(l-1)} + \frac{1}{x_0^2} \frac{(l+2)(l-1)}{(l+1)l} \right]. \quad (32)$$

## V. PULSAR TIMING

In the current pulsar-timing observation, radio pulses from an array of roughly 100 Galactic millisecond pulsars are being monitored with ground-based radio telescopes [3]. The redshift fluctuation of a pulsar in the pointing direction  $\mathbf{e}$  on the sky is given by

$$z(\mathbf{e}) = -\frac{1}{2} \int_{\eta_e}^{\eta_r} d\eta e^i e^j \frac{\partial}{\partial \eta} h_{ij}(\eta, \vec{x}), \quad (33)$$

where we have used  $\bar{z} = 0$  in Eq. (14) since the pulsar is in our Galaxy. The physical distance of the pulsar from us is  $D = \eta_r - \eta_e$ , which is of order 1 kpc. The quantity that is actually observed in the pulsar-timing observation is the time residual counted as

$$r(t) = \int_0^t dt' z(t'), \quad (34)$$

where  $t'$  denotes the laboratory time and  $t$  is the duration of the observation. Using the laboratory time  $t'$ , we rewrite Eq. (33) as

$$z(t', \mathbf{e}) = -\frac{1}{2} \int_{t'+\eta_e}^{t'+\eta_r} d\eta e^i e^j \frac{\partial}{\partial \eta} h_{ij}(\eta, \vec{x}). \quad (35)$$

Let us consider a SGWB with the narrow power spectrum (10), where  $H_*/M_p$  is the present GW amplitude. The wavenumber is assumed to be  $k_* \sim 10^6 \text{Mpc}^{-1}$ , lying within the pulsar-timing-array sensitivities to GWs

at nanohertz frequencies. At the present time, the GWs are traveling plane waves:

$$h(k_* \eta) \simeq \frac{H_*}{M_p} e^{-ik_* \eta}. \quad (36)$$

Then, we can construct the time-residual correlation between a pair of pulsars:

$$\begin{aligned} \langle r(t_1) r(t_2) \rangle &= \int_0^{t_1} dt' \int_0^{t_2} dt'' \langle z(t') z(t'') \rangle \\ &= \int_0^{t_1} dt' \int_0^{t_2} dt'' e^{-ik_*(t'-t'')} \langle z(\mathbf{e}_1) z(\mathbf{e}_2) \rangle. \end{aligned} \quad (37)$$

In Eq. (37), the integrand is simply the redshift fluctuation correlation,

$$\langle z(\mathbf{e}_1) z(\mathbf{e}_2) \rangle = \sum_l \frac{2l+1}{4\pi} C_l P_l(\mathbf{e}_1 \cdot \mathbf{e}_2), \quad (38)$$

whose power spectrum is given by

$$C_l \simeq \frac{H_*^2}{2\pi M_p^2} (l+2)(l+1)l(l-1) \left| \int_0^{x_1} dx e^{ix} \frac{j_l(x)}{x^2} \right|^2, \quad (39)$$

where  $x = k_*(\eta_r - \eta)$  and  $x_1 = k_* D \sim 10^3$ . Using the approximation in Eq. (31), we obtain an exact form for the power spectrum as

$$C_l \simeq \frac{2H_*^2}{\pi M_p^2} [(l+2)(l+1)l(l-1)]^{-1}. \quad (40)$$

In fact, this  $l^{-4}$  scaling has been derived using alternative methods [12]. Inserting the result (40) into the two-point correlation function (38) would give us the Hellings and Downs curve for the quadrupolar interpulsar correlations [13].

Recently, the NANOGrav Collaboration [14] has found strong evidence of a stochastic common-spectrum process across 45 millisecond pulsars, alluding to a SGWB with a characteristic strain of  $h_c = 1.92 \times 10^{-15}$  at a reference frequency of  $f_{\text{yr}} = 1 \text{yr}^{-1} \simeq 31.8 \text{nHz}$ . However, they have not found statistically significant evidence that this process has Hellings and Downs spatial correlations. If the SGWB is confirmed, its spectral energy density at  $f_{\text{yr}}$  can be read from Eq. (12) as

$$\begin{aligned} \Omega_{\text{GW}} h^2 &\simeq \frac{1}{6\pi^2} \frac{H_*^2}{M_p^2} \left( \frac{k_*}{100 \text{km s}^{-1} \text{Mpc}^{-1}} \right)^2 \\ &= \frac{2\pi^2}{3} h_c^2 \left( \frac{f_{\text{yr}}}{100 \text{km s}^{-1} \text{Mpc}^{-1}} \right)^2 \\ &\simeq 2.3 \times 10^{-9}, \end{aligned} \quad (41)$$

where  $|h(k_* \eta)| = H_*/M_p = \pi h_c$  and  $k_* = 2\pi f_{\text{yr}} \simeq 2.06 \times 10^7 \text{Mpc}^{-1}$ .

However, the exact form (40) underestimates the values of  $C_l$  at large  $l$ 's. In Fig. 1, we have plotted the power  $l(l+1)C_l$  against  $l$ , using the true value  $x_1 = 10^3$

to numerically evaluate the integral in Eq. (39). This is close to the Hellings and Downs power spectrum on large angular scales when  $l < 20$ , with  $C_l$  increased by 0.002%, 0.3%, 4.4%, 21.6%, 67.2% at  $l = 2, 10, 20, 30, 40$ , respectively. There exists a significant power at small scales when  $l \lesssim 10^3$ . It would be interesting to search for this small-scale power by measuring correlation between adjacent pulsars separated by about  $180^\circ/l \sim 0.2^\circ$  on the sky. For nearby pulsars with  $D \sim 0.1$  kpc, the exact form in Eq. (40) is no longer a good approximation, so one should use the full Eq. (39) to compute the power spectrum.

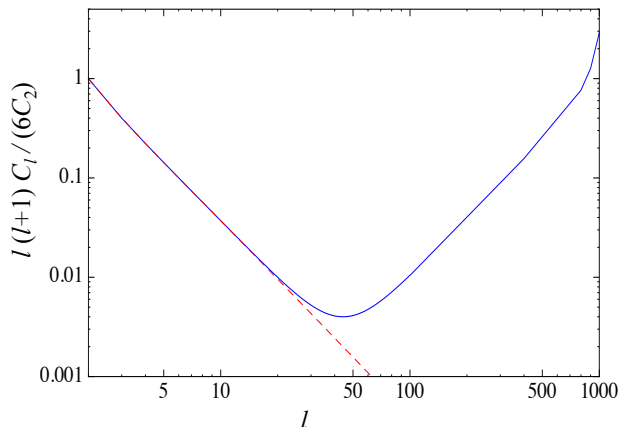


FIG. 1. Power spectra of the redshift fluctuation correlation. The dashed line is the Hellings and Downs power spectrum. The solid line is drawn from computing numerically Eq. (39) for  $x_1 = 10^3$ .

When we observe the pulsars at distance  $D$ , the angular separation between them for us to see the spatial fluctuation of GWs with wavelength  $\lambda$  is  $\lambda/D$ . This explains that  $C_l$  increases at small angular scales and peaks at  $l \sim 1000$  in Fig. 1. Also, the power spectrum is roughly a v-shape line standing at  $\log l \sim 1.5$  (or  $l \sim 40$ ), which separates between the large-scale power and the small-scale power. This is anticipated from the fact that the autocorrection has a power twice larger than the Hellings and Downs curve at zero lag (see, for example, Ref. [12]).

The integral in Eq. (39) is evaluated assuming that all the pulsars are at the same distance. However, in realistic observation they are spread out in distance. As such, the coherence will be lost, resulting in a suppression of the small-scale power. To assess the loss of coherence, let us consider a pair of pulsars with a sub-degree angular separation in a globular star cluster at distance of 1 kpc, noting that the size of a globular cluster ranges from a few pc to less than 0.1 kpc. Suppose one of the pulsar pair is nearer to us than the other one by  $\Delta x_1$ ; then, from Eq. (39) the fractional change in  $C_l$  will be given

by

$$\frac{\Delta C_l}{C_l} = - \left[ \int_{x_1 - \Delta x_1}^{x_1} dx e^{ix} \frac{j_l(x)}{x^2} \right] \left[ \int_0^{x_1} dx e^{ix} \frac{j_l(x)}{x^2} \right]^{-1}. \quad (42)$$

When  $x_1 = 10^3$  and  $\Delta x_1 = 1$  (giving  $\Delta D = 1$  pc),  $|\Delta C_l/C_l| < 1$  for  $l < 10^3$ , so the small-scale power still remains. When  $\Delta D$  increases to 10 pc,  $|\Delta C_l/C_l| < 1$  as long as  $l < 400$ . A search for this small-scale power in the current pulsar-timing observation is difficult due to poor statistics from a limited number of monitored pulsars on the sky. The future SKA project will observe about 6000 Galactic millisecond pulsars to reach a sensitivity three to four orders of magnitude better than the current pulsar-timing-array experiments [15]. It would be interesting to hunt for pulsar pairs in globular clusters to measure the correlation at small angular scales.

Furthermore, it would be interesting to consider extragalactic millisecond pulsars or other presumable cosmological precision clocks to measure the SGWB. In this case,  $\eta_r = \eta_0$  and  $\eta_e$  is the time of emission of light from the extragalactic sources at redshift  $\bar{z}$ . Assume  $\eta_e > \eta_*$ . Then, the redshift-fluctuation correlation function is enhanced by the redshift factor and reads

$$\langle \delta z(\mathbf{e}_1) \delta z(\mathbf{e}_2) \rangle = (1 + \bar{z})^2 \sum_l \frac{2l+1}{4\pi} C_l P_l(\mathbf{e}_1 \cdot \mathbf{e}_2). \quad (43)$$

Here  $C_l$  is given by Eq. (32) with  $x_1 = k_* D \gg 10^3$ , where  $D = \eta_0 - \eta_e$  is the comoving distance to the extragalactic sources.

## VI. CONCLUSION

We have revisited the Sachs-Wolfe gravitational effect of the stochastic gravitational wave background. Considering the effect as redshift-space fluctuations integrated along the line-of-sight from the observer to the observable, we have found that the line-of-sight integral is particularly useful for studying the imprint of short-wavelength gravitational waves on the CMB anisotropy, without having recourse to intensive numerical computations. The contribution of the short-wavelength gravitational waves to the large-scale CMB anisotropy  $C_l$  scales as  $l^{-4}$ . The integral can well be used to study the redshift fluctuations of millisecond pulsars. It reproduces the Hellings and Downs curve for the redshift correlation between a pair of distant pulsars. For nearby pulsars, we have calculated the deviation from the Hellings and Downs curve that should be taken into account in pulsar timing measurements.

## ACKNOWLEDGMENTS

This work was supported in part by the Ministry of Science and Technology (MOST) of Taiwan, Republic of China, under Grant No. MOST 109-2112-M-001-003.

- 
- [1] LIGO Scientific Collaboration and Virgo Collaboration: B. P. Abbott *et al.*, Phys. Rev. Lett. **116**, 061102 (2016).
- [2] LIGO Scientific Collaboration and Virgo Collaboration: B. P. Abbott *et al.*, Class. Quant. Grav. **37**, 055002 (2020).
- [3] For a review, see J. D. Romano, arXiv:1909.00269.
- [4] For a review, see M. Kamionkowski and E. D. Kovetz, Ann. Rev. Astron. Astrophys. **54**, 227 (2016).
- [5] For examples, see M. A. Sedda *et al.*, arXiv:1908.11375; V. Baibhav *et al.*, arXiv:1908.11390; J. Baker *et al.*, arXiv:1908.11410.
- [6] CMB-S4 Collaboration: K. Abazajian *et al.*, arXiv:2008.12619.
- [7] R. K. Sachs and A. M. Wolfe, Astrophys. J. **147**, 73 (1967).
- [8] L. F. Abbott and M. B. Wise, Nucl. Phys. **B244**, 541 (1984); K.-W. Ng, Int. J. Mod. Phys. A **11**, 3175 (1996).
- [9] A. A. Starobinsky, Pis'ma Astron. Zh. **11**, 323 (1985) [Sov. Astron. Lett. **11**, 133 (1985)]; K.-W. Ng and A. D. Speliotopoulos, Phys. Rev. D **52**, 2112 (1995).
- [10] Planck Collaboration: N. Aghanim *et al.*, Astron. Astrophys. **641**, A6 (2020).
- [11] T. Namikawa, S. Saga, D. Yamauchi, and A. Taruya, Phys. Rev. D **100**, 021303(R) (2019).
- [12] J. Gair, J. D. Romano, S. Taylor, and C. M. F. Mingarelli, Phys. Rev. D **90**, 082001 (2014).
- [13] R. W. Hellings and G. S. Downs, Astrophys. J. **265**, L39 (1983).
- [14] NANOGrav Collaboration: Z. Arzoumanian *et al.*, Astrophys. J. **905**, L34 (2020).
- [15] G. Janssen *et al.*, *Advancing Astrophysics with the Square Kilometre Array*, PoS AASKA14 (2015) 037.